ChemComm

COMMUNICATION

View Article Online
View Journal | View Issue

Check for updates

Cite this: *Chem. Commun.*, 2023, 59, 3898

Received 4th December 2022,
Accepted 7th March 2023

DOI: 10.1039/d2cc06598c

rsc.li/chemcomm

Published on 14 2023. Downloaded on 2025/7/25 4:41:11.

A hypoxia-activated photothermal agent inhibits multiple heat shock proteins for low-temperature photothermal therapy†

Xinhao Zhang, Shan-Shan Xue, Wei Pan,* Kaiye Wang, Na Li* and Bo Tang*

A near-infrared (NIR) organic photothermal agent (PTA) to inhibit three types of heat shock proteins (HSPs) was synthesized, which could be activated under hypoxic conditions for low-temperature photothermal therapy (PTT) of cancer.

Cancer phototherapy has been widely studied over the past few decades. Photodynamic therapy (PDT) is a traditional anticancer phototherapy in which the therapeutic effect relies on oxygen, but hypoxia is a common microenvironment feature of most tumors.[1] As an oxygen-independent therapy, photothermal therapy (PTT) has drawn increasing attention of researchers. Photothermal agents (PTAs) have been used to effectively convert light into localized heat to damage tumor tissue in PTT.[2] Among the existing PTAs, organic PTAs have drawn broad attention because of their excellent biodegradability, good biocompatibility, and structural diversity.[3] To date, considerable efforts have been dedicated to the progress of efficient organic PTAs for promoting the PTT effect.[4] Due to the thermal resistance of tumors, high power irradiation in PTT was indispensable to realize the hyperthermia effect for tumor ablation.[5] However, using the high power density of lasers to achieve valid PTT may damage the normal tissues near the tumor and cause inflammation.[6] It is still a big challenge to develop effective organic PTAs against tumor thermal resistance in low-temperature (40–45 °C) PTT.

Heat shock proteins (HSPs) are generated in cells and protect other proteins from heat damage under the process of hyperthermia.[7] During the PTT process, overexpression of HSPs could be induced by heat stressor, which is the main reason for the thermal resistance of tumors.[8] The thermal resistance may alleviate the PTT effect or even result in recurrence of cancer.[9] Thus, the inhibition of HSPs could certainly enhance the therapeutic effect of PTT.[10] Considering that the HSP family is composed of several kinds of HSPs, the efficiency of PTT was limited by the single-HSP inhibition strategy. As a type of signal transduction protein, extracellular signal-regulated kinase (ERK) plays an important role in cell signalling, which has been proved to be closely related to the expression of HSPs.[11] The expression of HSPs is dependent on ERK phosphorylation, which means the inhibition of the ERK phosphorylation pathway may significantly reduce the expression of several kinds of HSPs.[12,13] It is desirable to develop a suitable PTA for restraining the activation of ERK, by which multi-HSP expression will be inhibited and the thermal resistance of the tumor will be further reduced.

In this study, an NIR organic PTA, denoted as E-Cy-NB, was developed for inhibiting multiple HSPs and activating under hypoxic conditions for low-temperature PTT. Cyanine dye (IR825) was employed as a photothermal fluorophore because it exhibits excellent photophysical properties and low biotoxicity.[14] (*Z*)-3-(2-aminoethyl)-5-(4-ethoxybenzylidene)thiazolidine-2,4-dione (ERK pathway inhibitor group) and 4-nitrobenzyl carbonochloridate (nitroreductase (NTR) activation group) were further connected to produce the final molecule. Under hypoxic tumor conditions, E-Cy-NB could be converted by overexpressed NTR (the level of NTR is positively correlated with hypoxic conditions)[15] to another molecule, E-Cy-AB (see Scheme S3, ESI†). Compared with E-Cy-NB, the photothermal effect of E-Cy-AB was enhanced due to the non-radiative relaxation deactivation pathway, which was beneficial for photothermal conversion. Linked with the ERK pathway inhibiting group,[16] the PTA can restrain the phosphorylation of ERK 1/2 (two closely related proteins) to inhibit the ERK pathway, which is the key for suppressing the expression of multiple HSPs. Under NIR irradiation, the low-temperature PTT apoptosis was induced by E-Cy-AB. Thus, this organic PTA could realize low-temperature PTT under NIR irradiation through inhibition of multi-HSP expression

College of Chemistry, Chemical Engineering and Materials Science, Key Laboratory of Molecular and Nano Probes, Ministry of Education, Collaborative Innovation Center of Functionalized Probes for Chemical Imaging in Universities of Shandong, Institute of Molecular and Nano Science, Shandong Normal University, Jinan 250014, P. R. China. E-mail: panwei@sdnu.edu.cn, lina@sdnu.edu.cn, tangb@sdnu.edu.cn

† Electronic supplementary information (ESI) available: Detailed experimental procedures and supporting figures. See DOI: https://doi.org/10.1039/d2cc06598c

This journal is © The Royal Society of Chemistry 2023

Published on 14 2023. Downloaded on 2025/7/25 4:41:11.

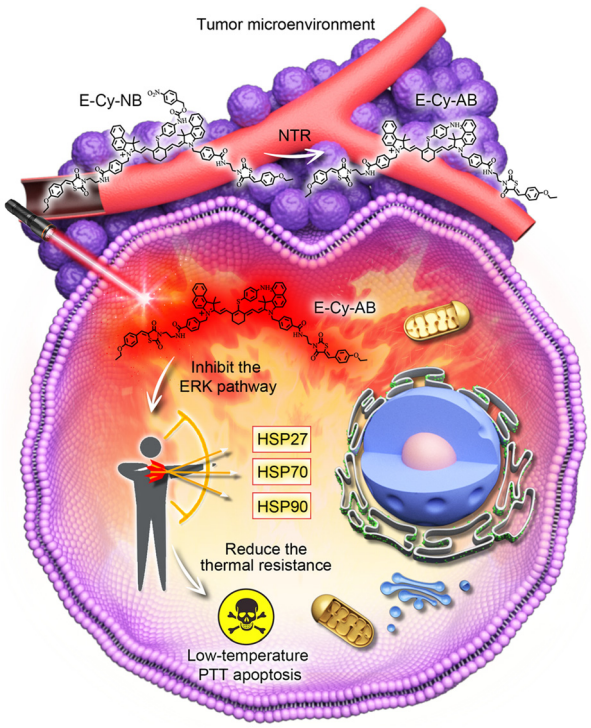

Scheme 1 Schematic illustration of E-Cy-NB/E-Cy-AB for low-temperature PTT.

and activation in the hypoxic microenvironment of the tumor (Scheme 1).

The cyanine dye (red part in Fig. 1), IR825, was synthesized as the photothermal fluorophore framework.[14] The inhibiting moiety of the ERK pathway (blue part in Fig. 1) was synthesized in 3 steps and covalently linked to IR825 through the amido bond. The product reacted with 4-aminothiophenol *via* a substitution reaction and further linked with nitrobenzyl methyl ester (purple part in Fig. 1) to obtain the final molecule E-Cy-NB (Fig. 1). The E-Cy-NB, Cy-NB (without the ERK inhibited group) and the other compounds were characterized using high resolution mass spectrometry (HRMS) and nuclear magnetic resonance (NMR) (Fig. S1–S8, ESI†).

First, we verified the transformation from E-Cy-NB to E-Cy-AB. As we know, NTR could reduce the nitro-containing group in the presence of NADH, which were both overexpressed in the hypoxic tumor environment.[15] When the E-Cy-NB solution

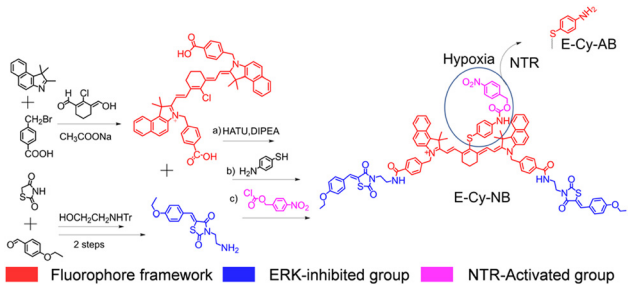

Fig. 1 Synthetic procedure of the PTA (E-Cy-NB).

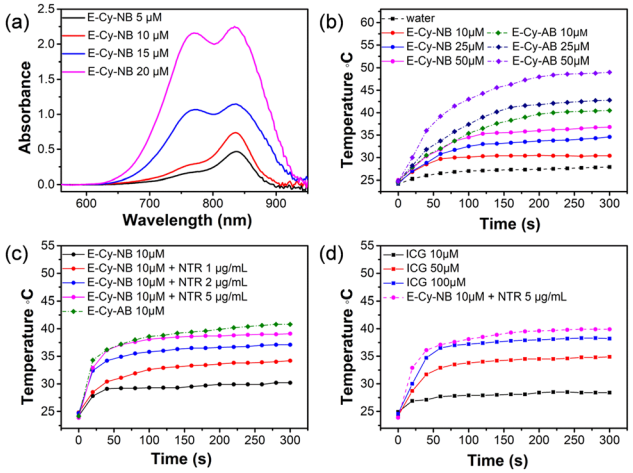

Fig. 2 (a) UV-vis absorbance spectra of E-Cy-NB in CH_3OH. (b) The heating curves of E-Cy-NB/E-Cy-AB with different concentrations. (c) Temperature changes of E-Cy-NB solutions (10 μM) after treatment with NTR, and the temperature of E-Cy-AB (10 μM) under an 808 nm laser. (d) The temperature changes of E-Cy-NB/E-Cy-AB and ICG with different concentrations under an NIR laser (808 nm, 0.33 W cm^{-2}).

(DMSO/water, v/v = 1 : 9) was treated with NTR (5 μg mL^{-1}) and NADH (350 μg mL^{-1}), the HRMS spectra of the resulting solution showed a new peak (*m*/*z*: 1461.5644), which matched well with E-Cy-AB (calculated *m*/*z*: 1461.5478) (Fig. S9a–c, ESI†). Besides, the activation of NTR to E-Cy-NB was confirmed by fluorescence emission spectroscopy. Under the same conditions, the fluorescence intensity of E-Cy-NB solution was gradually decreased. After 60 min, the fluorescence intensity of the above solution was consistent with that of E-Cy-AB (Fig. S10, ESI†). These results suggest that E-Cy-NB could be converted to E-Cy-AB in the presence of NTR.

The photophysical properties of E-Cy-NB were tested. As shown in Fig. 2a and Fig. S11 (ESI†), the UV-vis spectra of E-Cy-NB were recorded in DMSO/water (v/v = 1 : 9) solution, and the intensity increased with the increase of the concentration of PTA. The solution was exposed to an 808 nm laser for 24 h and no obvious change in the absorption was observed, which confirmed the photostability of E-Cy-NB (Fig. S12, ESI†). To verify the PDT effect, the singlet oxygen generation of PTA was investigated.[17] The singlet oxygen quantum yield of E-Cy-NB/Cy-NB was calculated to be 0.51/0.30, which highlights that the attachment of the ERK inhibitor significantly enhances the ROS generated upon irradiation, and that these agents have a significant PDT effect (see more details in the ESI† and Fig. S13 and S14). According to the American National Safe Standard of 808 nm irradiation (ANSI Z136.1-2007),[18] the 0.33 W cm^{-2} power density was employed for PTAs in the following experiments to maximize the photothermal capability and avoid side effects. The temperature of PTAs gradually increased with the concentration under NIR irradiation (Fig. 2b). Under the same conditions, the temperature of E-Cy-AB was much higher than that of E-Cy-NB. Upon NIR irradiation, the temperature of E-Cy-NB solutions increased as the concentration of NTR increased from 0 to 5 μg mL^{-1} and

Published on 14 2023. Downloaded on 2025/7/25 4:41:11.

was gradually close to that of E-Cy-AB (*ca.* 41 °C) (Fig. 2c). The results indicated that E-Cy-NB possessed enough PTT ability for low-temperature PTT under hypoxic tumor conditions. Compared with indocyanine green (ICG, a commercially available PTA) the photothermal temperature of ICG (100 μM) was lower than that of E-Cy-AB (10 μM) under the same irradiation conditions (Fig. 2d). After three laser on/off cycles, the maximum photothermal temperature of E-Cy-AB was nearly the same (Fig. S15, ESI†), indicating the good photothermal stability of E-Cy-AB. Based on the above experimental results and Fig. S16 (ESI†), the photothermal conversion efficiency of E-Cy-AB was calculated to be 35.36% (see the ESI† for details).

To verify the cell permeability of PTAs (E-Cy-NB/Cy-NB/Cy), confocal imaging and fluorescence activated cell sorting (FACS) experiments were performed. As shown in Fig. S17–S19 (ESI†), after being co-incubated with different PTAs, most of the agents stayed in 4T1 cells. The results indicated that PTAs could be readily taken up by 4T1 cells. To determine the cytotoxicity of E-Cy-NB, the MTT assay was performed. 4T1 cells were treated with various concentrations of E-Cy-NB with or without NIR laser irradiation. As expected, E-Cy-NB showed notable cytotoxicity to 4T1 cells with increasing concentration of E-Cy-NB under exposure to an 808 nm NIR laser (0.33 W cm^{-2}, 300 s) (Fig. S20a, ESI†). The half-maximum inhibitory concentration (IC_{50}) value of 4T1 cells treated with E-Cy-NB was calculated to be 5.4 μM under hypoxic conditions, which is much lower than that of ICG (76.0 μM) (Fig. S20b, ESI†). Considering safety and photothermal efficiency, 10 μM PTA was used in the following experiments. The results suggested that our PTA possessed good phototoxicity under hypoxia, which is much better than that of ICG. In order to validate the HSP-inhibiting capability of E-Cy-NB, the western blotting (WB) analysis was performed using GADPH as a control protein. According to Fig. 3a and Fig. S21 (ESI†), the expression of HSPs in the NIR group was greatly increased, while that in the E-Cy-NB + NIR group was notably reduced. Meanwhile, the levels of HSPs in 4T1 cells treated with E-Cy-NB were much lower than those in the PBS group. But barely no decrease in the HSP quantity was observed in both Cy-NB + NIR and Cy-NB groups, which suggested that Cy-NB cannot suppress HSPs. Furthermore, in immunofluorescence analysis, the green fluorescence intensity was positively correlated to the HSP levels. According to Fig. 3b, the green fluorescence intensity of the E-Cy-NB + NIR and E-Cy-NB groups was lower than that of NIR and PBS groups, respectively. The immunofluorescence analysis showed results consistent with the WB analysis results described above. To study the inhibition of the ERK pathway, changes in the *p*-ERK 1/2 protein levels (main phosphorylation product of the ERK pathway) were detected using WB analysis after different treatments (Fig. S22, ESI†). Under NIR irradiation, the phosphorylation of the ERK pathway was aggravated and the expression of *p*-ERK 1/2 proteins was increased. However, the levels of *p*-ERK 1/2 proteins were reduced after treatment with E-Cy-NB contrast in the control group. The above experimental results indicated that E-Cy-NB could effectively realize multi-HSP inhibition through suppressing the activation of the ERK pathway. Calcein-AM/PI-stained assay experiments were performed to confirm the PTT effect of the PTAs. As shown in Fig. S25 (ESI†), a significant red signal was observed in the fluorescence image of the E-Cy-NB + NIR group. Under the hypoxic environment, 4T1 cells were treated with E-Cy-NB, and nearly no live cells can be seen after NIR irradiation because the level of NTR was increased. This indicates that E-Cy-NB displayed good photo-cytotoxicity, especially in hypoxia. ICG showed a slightly weaker red signal even after using an amount that is 10 times more than that of E-Cy-NB under the same irradiation conditions. Moreover, a notable green signal was observed in the fluorescence image of 4T1 cells treated without NIR laser irradiation (Fig. S25, ESI†). The results of the flow apoptosis experiment (Fig. S26, ESI†) were consistent with the fluorescence confocal images of the Calcein-AM/PI-stained assay. Besides, the apoptosis rate of 4T1 cells was slow in the E-Cy-NB + NIR + DIC (dicoumarin, a known NTR inhibitor) group due to the inhibition of NTR. All these results indicated that E-Cy-NB exerted a great PTT effect under the hypoxic environment and good biosafety.

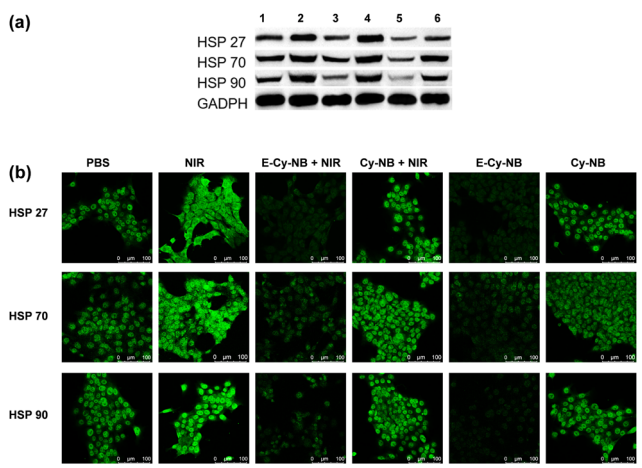

Fig. 3 (a) Western blot images (1: PBS, 2: NIR, 3 : 10 μM E-Cy-NB + NIR, 4 : 10 μM Cy-NB + NIR, 5 : 10 μM E-Cy-NB and 6 : 10 μM Cy-NB) for 8 h. (b) Immunofluorescence analysis of HSP levels in 4T1 cells after different treatments.

To confirm the much better therapeutic effect of the multi-HSP-inhibited strategy, the MTT assay was performed using PES (2-phenylethynesulfonamide, an HSP70 inhibitor) and GA (gambogic acid, an HSP90 inhibitor), since HSP70 and HSP90 were frequently studied due to their common expression in cells. As the fluorescence part of E-Cy-NB, IR825 was chosen to be the PTA to combine the molecular inhibitor of HSP for the synergistic therapy. The results are shown in Fig. S27 (ESI†); the survival rate of 4T1 cells treated with IR825 + PES/IR825 + GA/IR825 + PES + GA was higher than those treated with E-Cy-NB under the same conditions, which indicated that the multi-HSP-inhibited strategy was more effective than the single HSP-inhibited strategy.

Encouraged by the effective photothermal effects of E-Cy-NB *in vitro*, the 4T1 breast tumor bearing BALB/c mouse models were established to assess the treatment effect of E-Cy-NB under low NIR density (Fig. 4a). Seven groups of mice were

 This journal is © The Royal Society of Chemistry 2023

Published on 14 2023. Downloaded on 2025/7/25 4:41:11.

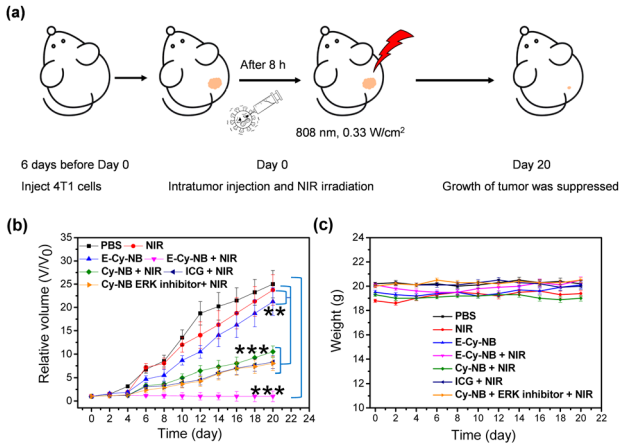

Fig. 4 (a) Cancer therapy of 4T1 tumor-bearing mice. (b) Tumor growth curves of mice in different groups (mean: SD, $n = 5$, $^{**}P < 0.01$, $^{***}P < 0.001$). (c) The change of body weight in each mouse group.

randomly set and intratumorally injected with different treatments. The measurement of temperature in the tumor area was performed during the PTT treatment. The results demonstrated that the temperature of the PTA group increased rapidly under NIR irradiation (Fig. S28, ESI†). As shown in Fig. S30 (ESI†) and Fig. 4b, barely no tumor inhibition effect was observed in the NIR group. The volumes of tumors in the E-Cy-NB group were close to those in the PBS group. Remarkably, the tumor growth in the group treated with E-Cy-NB + NIR showed considerable suppression compared with the other groups owing to the excellent inhibition of HSPs and the PTT effect, while the volumes of tumors in the other groups (treated with Cy-NB and ICG under laser irradiation) were slightly smaller than those in the PBS group. Compared with the E-Cy-NB + NIR group, the Cy-NB + ERK inhibitor + NIR group exhibited a significantly weaker effect on the tumors. The difference between these groups can be rationalized by the enhanced production of singlet oxygen by E-Cy-NB *vs.* Cy-NB leading to a greater PDT effect. The weights of all mice were in the normal range (Fig. 4c). The histological hematoxylin-eosin (H&E) staining experiment was carried out (Fig. S31, ESI†), and the results indicate that the tumor tissue treated with E-Cy-NB under NIR irradiation showed a largely necrotic area than that in the PBS group. Furthermore, the H&E staining images reveal that all the major organs displayed no noticeable pathological damage. After that, the tests of blood routine and serum biochemical indicators were proceeded to assess the biosafety of PTA. All the values were in the normal range (Fig. S32, ESI†). The above experimental results indicated that E-Cy-NB had high biosafety and could realize perfect tumor inhibition in PTT.

In summary, a multi-HSP-inhibited PTA (E-Cy-NB) was successfully developed for low-temperature PTT. E-Cy-NB could restrain the phosphorylation of the ERK pathway and further effectively inhibited the overexpression of HSP27, HSP70, and HSP90 to reduce the thermal resistance of the tumor under the PTT process. In the NTR-activated group, this PTA showed great photothermal performance under the hypoxic tumor microenvironment with low NIR irradiation, while the therapeutic effect was obviously reduced under normoxic conditions. The *in vivo* experimental results indicated that E-Cy-NB could effectively inhibit tumor growth with irradiation in 4T1 bearing BALB/c mice models. Our work provided a potential low-temperature PTT strategy and an inspirational approach for more effective HSP-inhibited PTAs.

This work was supported by Shandong Provincial Key Research and Development Program (Major Scientific and Technological Innovation Project) (2021CXGC010515), National Natural Science Foundation of China (22274089), Youth Innovation Science and Technology Program of Higher Education Institution of Shandong Province (2021KJ030) and Jinan Innovation Team (2021GXRC034).

Conflicts of interest

The authors have declared that no competing interest exists.

Notes and references

1 M. Li, J. Xia, R. Tian, J. Wang, J. Fan, J. Du, S. Long, X. Song, J. W. Foley and X. Peng, *J. Am. Chem. Soc.*, 2018, **140**, 14851–14859.
2 S. Zhao, L. Yan, M. Cao, L. Huang, M. Lan and W. Zhang, *ACS Appl. Mater. Interfaces*, 2021, **13**, 53610–53617.
3 M. Shi, *et al.*, *Angew. Chem., Int. Ed.*, 2021, **60**, 13564–13568.
4 H. S. Jung, *et al.*, *Chem. Soc. Rev.*, 2018, **47**, 2280–2297.
5 G. Gao, X. Sun, X. Liu, Y. W. Jiang, R. Tang, Y. Guo, F. G. Wu and G. Liang, *Adv. Funct. Mater.*, 2021, **31**, 210283.
6 Y. Cao, *et al.*, *ACS Nano*, 2019, **13**, 1499–1510.
7 X. He, *et al.*, *Nano Today*, 2021, **39**, 101174.
8 G. Zhang, C. Xu and J. Li, *J. Nanobiotechnol.*, 2021, **19**, 9.
9 K. Mori, *et al.*, *J. Clin. Oncol.*, 2017, **35**, 546.
10 G. Gao, *et al.*, *Adv. Funct. Mater.*, 2020, **30**, 1909391.
11 D. C. H. Ng and M. A. Bogoyevitch, *J. Biol. Chem.*, 2000, **275**, 40856–40866.
12 J. M. Keller, *et al.*, *Comp. Biochem. Physiol., Part A: Mol. Integr. Physiol.*, 2018, **150**, 307–314.
13 S. Yang, *et al.*, *Cell Stress Chaperones*, 2021, **26**, 173–185.
14 L. Cheng, W. He, H. Gong, C. Wang, Q. Chen, Z. Cheng and Z. Liu, *Adv. Funct. Mater.*, 2013, **23**, 5893–5902.
15 X. Zhao, S. Long, M. Li, J. Cao, Y. Li, L. Guo, W. Sun, J. Du, J. Fan and X. Peng, *J. Am. Chem. Soc.*, 2020, **142**, 1510–1517.
16 S. Fletcher, *et al.*, *Org. Biomol. Chem.*, 2013, **11**, 3706–3732.
17 Y. Zou, J. Du, J. Fan and X. Peng, *Small*, 2020, **16**, 1907677.
18 X. Ding, C. H. Liow, M. Zhang, R. Huang, C. Li, H. Shen, M. Liu, Y. Zou, N. Gao, Z. Zhang, Y. Li, Q. Wang, S. Li and J. Jiang, *J. Am. Chem. Soc.*, 2014, **136**, 15684–15693.